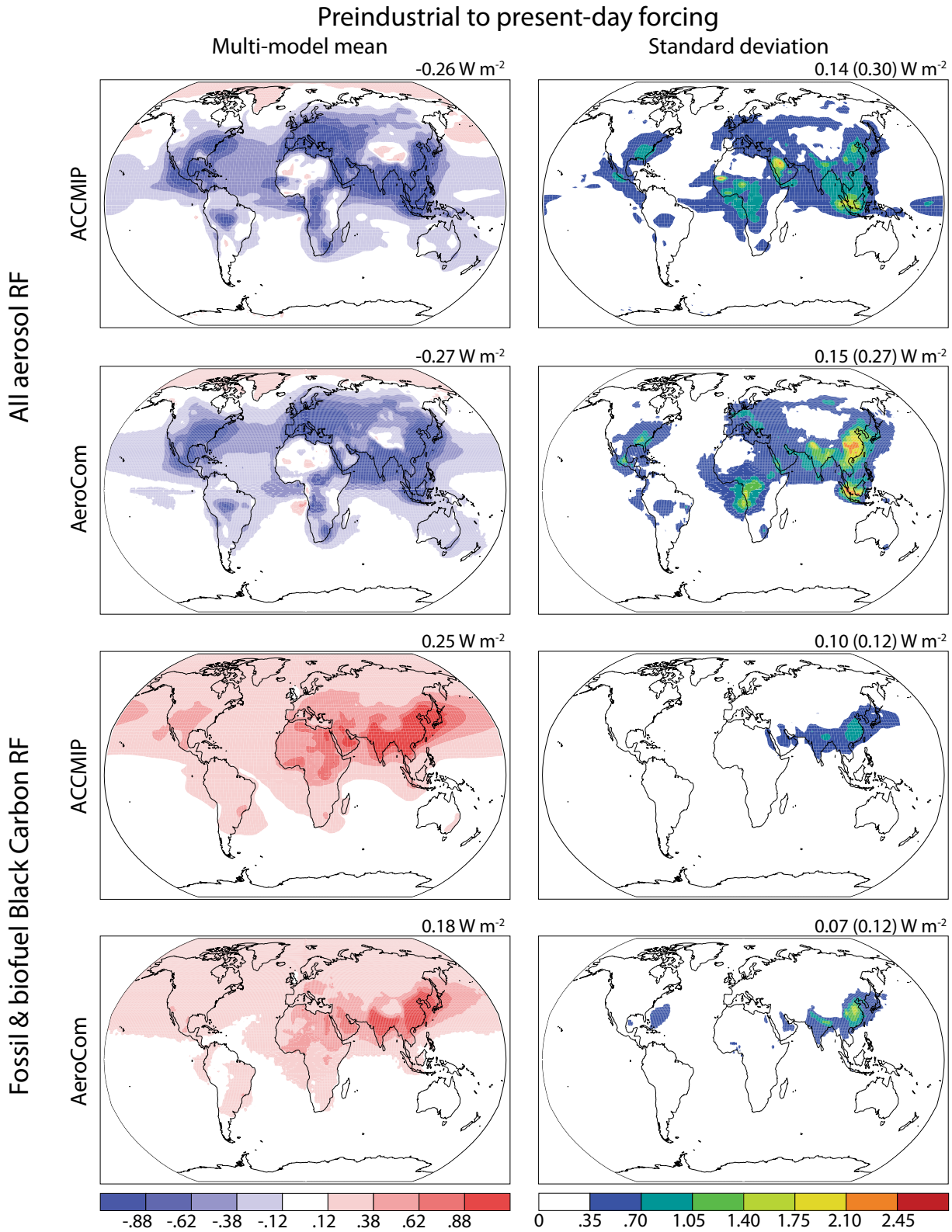

Figure 8.24 | Spatial pattern of ACCMIP and 16 AeroCom models 1850 to 2000 RF due to aerosol–radiation interaction, mean values (left) and standard deviation (right). Note that different carbonaceous aerosol diagnostics are used here compared to Figure 8.23, due to available AeroCom fields. Values above are the average of the area-weighted global means, with the area weighted mean of the standard deviation of models at each point provided in parentheses.

8.6.2 Spatial Evolution of Radiative Forcing and Response over the Industrial Era

8.6.2.1 Regional Forcing Changes During the Industrial Era

The spatial distribution of the WMGHG RF has shifted only slightly over the industrial period; however the RF spatial distributions for NTCFs has shifted with emissions, due to the timing of regional development and implementation of pollution standards (Supplementary Material Figures 8.SM.1 and 8.SM.2 show regional trends and emissions maps; Lamarque et al., 2013). Figure 8.25 shows how the distributions of aerosol and ozone forcings are modelled to have changed up to 1930, 1980 and 2000. Substantial industrial coal-burning in the early part of the 20th century occurred in the northeastern United States and Western Europe, leading to stronger sulphate and BC forcing near those regions (Figure 8.25, left). Between 1950 and 1970, coal burning for power generation increased while coal burning for other purposes was replaced by oil and natural gas and motor vehicle usage grew rapidly in these regions, leading to more sulphate and less BC. Peak aerosol forcing in North America and Europe occurred around 1970–1980 (Figure 8.25, second column), while Asian development led to increased biofuel and fossil fuel sources of aerosols and ozone precursors toward the end of the century. During the final decades of the century, desulphurization controls reduced sulphur emissions from North America and Europe, resulting in reduced negative forcing in these regions and positive Arctic aerosol forcing. The SH ozone hole developed during the final three decades, with negative forcing over high latitudes. Biomass burning generated ozone and carbonaceous aerosols in NH high-latitudes early in the century, with increased tropical burning from mid to late century.

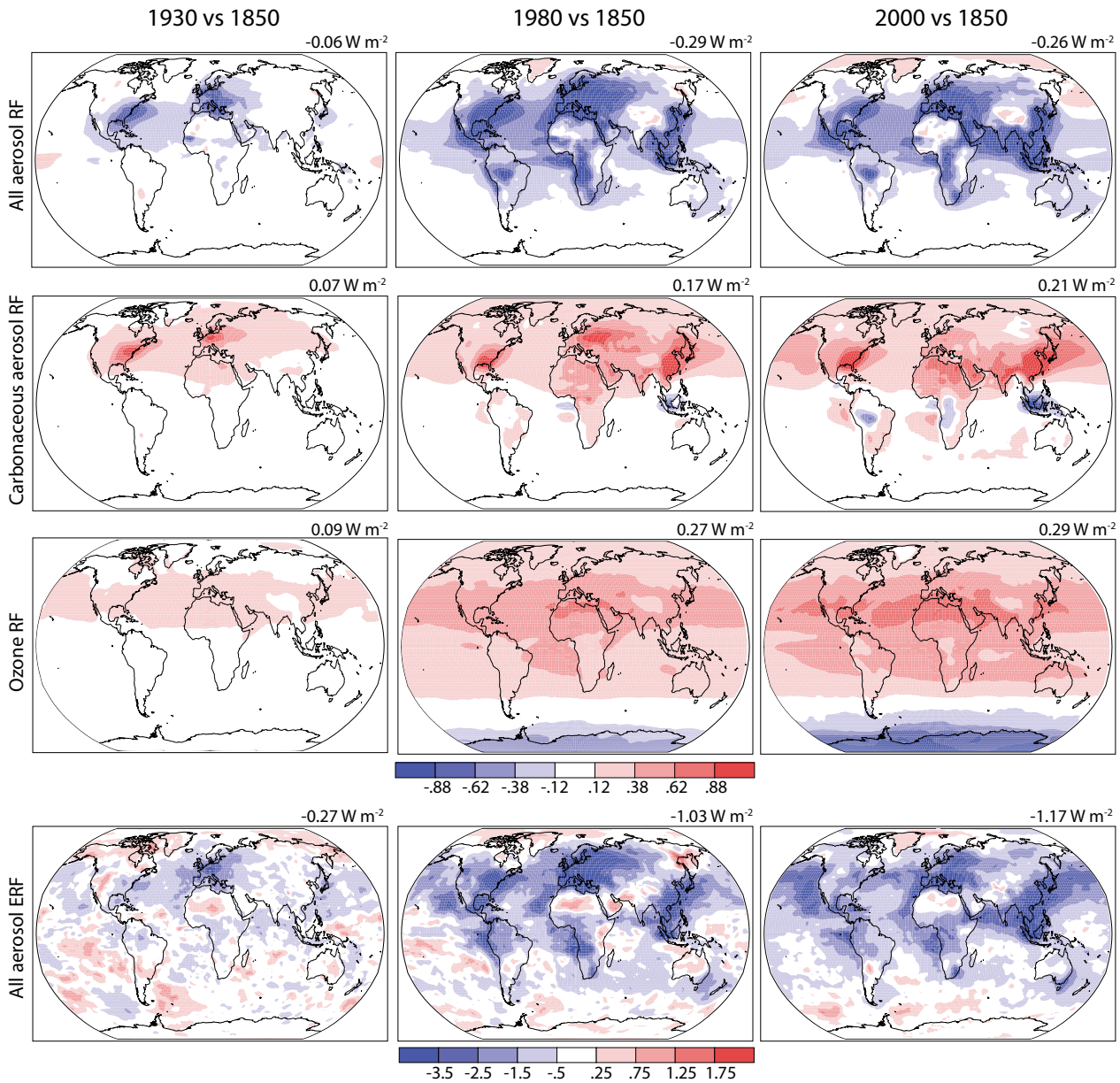

Figure 8.25 | Multi-model mean RF due to aerosol–radiation interaction of all aerosols, carbonaceous aerosols, ozone, and aerosol ERF (W m^{-2}) for the indicated times based on the ACCMIP simulations. Global area-weighted means are given in the upper right.

Aerosol ERF grew rapidly from 1930 to 1980, as did RF due to aerosol–radiation interaction, with a spatial structure reflecting both the influence of aerosol–radiation and aerosol–cloud interactions that are especially strong over pollution outflow regions and over areas with high surface albedo. From 1980 to 2000, aerosol ERF continued to become more negative even as negative RF due to aerosol–radiation interaction grew weaker, with the spatial pattern showing strengthening of aerosol ERF over Asia and weakening of aerosol ERF over North America and Europe.

Soil dust has changed since the pre-industrial due to land disturbance and resulting desertification (a forcing) and to changes in climate (a feedback). Mahowald et al. (2010) showed approximate doubling in dust loading over the 20th century (–0.1 W m^{-2}; consistent with the best estimate in Section 7.5.2; Section 8.3.4.2), primarily from the Saharan and Middle Eastern Deserts, with largest increase from the 1950s to the 1980s (–0.3 W m^{-2}), followed by a leveling. The increased dustiness reduces model precipitation within the Saharan source region, improving agreement with observed precipitation.

Aerosol loading changes during the past century have impacted radiation at the surface (Section 2.3.3), with peak radiation reductions in North America and Europe in the 1980s, and ongoing reduction in South and East Asia (Wild, 2009). The AR4 and CMIP5 models simulated these trends but underestimated their magnitude, the decadal temperature variations and the diurnal temperature range over land (Wild, 2009; see Chapter 9).

Changes in spatial patterns of species and their forcing over the century are difficult to validate due to sparse observations of short-lived species. Some constraint comes from limited historical observations in ice core records and from shorter trends beginning in late century from satellite and surface-based site measurements. The emissions estimates for historical species are very uncertain, especially for carbonaceous aerosols and dust. Therefore, the *confidence* in the historical forcing pattern changes is *low* for RF due to aerosol–radiation interaction and ozone, and *very low* for ERF, carbonaceous aerosols and dust.

8.6.2.2 Relationship Between Regional Forcing Patterns and Climate Response During the Industrial Era

An increasing body of research considers how spatial variations in RF affect climate response. Detection and attribution methods have had limited success in discerning statistically significant regional climate signals from regional forcing, due to large internal climate variability at regional scales, uncertainty in model processes and sparse regional observational records (Chapter 10). Meanwhile, research including model sensitivity studies for NTCFs, which vary strongly in space in time, explores climate response patterns.

In AR4 (Forster et al., 2007; Knutti et al., 2008) it was argued that the spatial pattern of forcing is not indicative of the pattern of climate response. Rather, the response is linked more closely to TOA flux resulting from the climate feedback spatial patterns (Boer and Yu, 2003; Taylor et al., 2011; Ming and Ramaswamy, 2012), with the lapse rate, surface albedo and cloud feedbacks explaining most of the temperature response. Yet Crook and Forster (2011) showed that both the spatial distribution of climate feedbacks and of heterogeneous forcing played important roles in the patterns of 20th century temperature changes. Other studies since AR4 have probed relationships between forcing patterns and climate responses.

Broad links between forcing and climate response have been identified. Shindell et al. (2010) used multiple models to show that surface temperature changes are much more sensitive to latitudinal than longitudinal variations in forcing. Shindell and Faluvegi (2009) used a model inverse approach to infer that NH aerosol reduction was associated with more than 70% of Arctic warming from the 1970s to the 2000s, and that Arctic and much of the SH surface temperature changes are strongly affected by remote forcing changes (alsoSection 10.3.1.1.4). Voulgarakis and Shindell (2010) defined a regional transient temperature sensitivity parameter, or temperature response per unit forcing for each 4-degree latitude band. Using observed surface air temperature changes they showed that the parameter is best constrained from 50°S to 25°N, where the value is 0.35°C (W $m^{-2})^{-1}$, smaller than at northern higher latitudes, and 35% smaller than in AR4 models.

Some aerosol model studies have demonstrated highly localized climate response to regional forcing. Significant regional cooling and hydrological shifts in the eastern USA and in Eastern Asia during the last half of the 20th century were modelled and attributed to local aerosols (Leibensperger et al., 2008, 2012a, 2012b; Chang et al., 2009) and localized warming projected for aerosol reductions (Mickley et al., 2012). Observations have also linked historical trends in aerosols and temperature (Ruckstuhl et al., 2008; Philipona et al., 2009).

Since AR4, there has been new research on aerosol influences on the hydrologic cycle (also Sections 7.4, 7.6.4, 10.3.3.1 and 11.3.2.4.3). Increased aerosol loading, with greater surface energy flux reduction in the NH, has been implicated in the observed southward shift of the Intertropical Convergence Zone (ITCZ) towards the hemisphere with smaller surface energy reduction: southward up to the 1980s with a reversal since (e.g., Denman et al., 2007; Zhang et al., 2007). Several studies have modelled an associated reduction in NH precipitation and associated shifts in the Hadley circulation (e.g., Rotstayn et al., 2000; Williams et al., 2001; Ming et al., 2011). The ITCZ shift may in turn be responsible for broad regional precipitation changes, including drying of the Sahel (e.g., Rotstayn and Lohmann, 2002; Biasutti and Giannini, 2006; Kawase et al., 2010; Ackerley et al., 2011) and northwestern Brazil (Cox et al., 2008), both of which peaked in the 1980s. These hemispheric asymmetric ITCZ effects are overlaid on thermodynamic aerosol effects which moisten subtropical regions, countering GHG-induced drying of these regions (Ming et al., 2011). Studies indicate that aerosols are more effective than an equivalent WMGHG forcing for shifting precipitation, and that historical trends in several areas cannot be explained without including aerosol forcing (Bollasina et al., 2011; Booth et al., 2012; Shindell et al., 2012a; Shindell et al., 2012b). However, *confidence* in attribution of any human influence on zonal shifts in precipitation distribution is only *medium* (Section 10.3.2.2).

There is increasing evidence but limited agreement that absorbing aerosols influence cloud distributions (Section 7.3.4.2). Absorbing

aerosols apparently have complex influences on precipitation in monsoon regions. Model studies of Stephens et al. (2004) and Miller et al. (2004) showed that dust absorption over Africa enhances low-level convergence, vertical velocities and therefore local monsoon circulation and precipitation. On the other hand, Kawase et al. (2010) showed that biomass burning BC may cause the decreasing precipitation trend seen in tropical Africa during austral summer, due to reduction in evaporation and enhanced subsidence. The aerosol effects on the Indian monsoon are similarly complex, and have been the subject of numerous studies (e.g., Ramanathan et al., 2005; Chung and Ramanathan, 2006; Lau et al., 2006; Wang et al., 2009; Bollasina et al., (2011), but a clear picture of how the regional aerosol forcing correlates with responses has not yet fully emerged. Attribution of changes in monsoon to human influence generally has *low confidence* (Section 10.3).

Stratospheric ozone loss modelling has demonstrated an effect on the SH stratosphere similar to increased GHGs, cooling stratospheric temperatures, strengthening the polar vortex and shifting the westerly jet poleward; however causing cooler Antarctic surface temperatures, with larger influence on austral summer conditions (Son et al., 2009; McLandress et al., 2011; Thompson et al., 2011; see also Sections 10.3.3 and 11.3.2.4.3.) In the troposphere, models indicate that increased tropospheric ozone has caused warming, proportionally more in the NH and notably to the Arctic during winter, mainly during the second half of the 20th century (Shindell et al., 2006a).

Albedo changes due to land use and land cover changes exert a heterogeneous climate forcing (Figure 8.9). The surface albedo brightened on the one hand due to a shift from forest to brighter croplands, causing local cooling (e.g., Eliseev and Mokhov, 2011; Lee et al., 2011), but also darkened due to the re-expansion of forests to higher latitudes (Esper and Schweingruber, 2004) and increased vegetation height in snowy regions (Bonfils et al., 2012; also Section 8.3.5). Model studies have shown cooling from land use and land cover changes, especially over NH continents, although without demonstrating a detectable signal in observations (Matthews et al., 2004).

In addition to land use and climate-induced vegetation changes, CO_2 affects vegetation forcing indirectly, reducing transpiration from plants as stomata open less with increasing CO_2, resulting in localized atmospheric drying and warming (Section 11.3.2.3.1; Joshi and Gregory, 2008). These are not included in the standard RF (Section 8.1) and may be considered feedbacks (Section 8.3.2). This is modelled to be largest over the Amazon, the central African forest, and to some extent over boreal and temperate forests (Andrews et al., 2011). In the coupled climate modelling study of Lawrence and Chase (2010), the vegetation changes caused significant reduction in evapotranspiration, drying and warming in tropical and subtropical regions, with insignificant cooling at higher latitudes. Overall, vegetation changes may have caused modest cooling at high latitudes and warming at low latitudes, but the uncertainties are large and *confidence* is *very low*.

Deposition of BC on snow and ice, and loss of snow and ice darken the surface, reduces albedo, and enhances climate warming. Substantial snow-cover reduction of North America leads to warmer North American summertime temperature in models having a strong snow albedo feedback. These forcings can also have non-local impacts that result from enhanced land-ocean temperature contrast, increasing surface convergence over land and divergence over oceans. A poleward intensification of the high pressure patterns and subtropical jet may also result (Fletcher et al., 2009). BC contributions to snow darkening reduces snow cover, however the magnitude of the effect is very uncertain (see Sections 7.5.2.3 and 8.3.4.4). A model study calculated BC-albedo reduction to cause about 20% Arctic snow/ice cover reduction and 20% of Arctic warming over the previous century (Koch et al., 2011). However, reductions in Arctic soot during the past two decades (e.g., Hegg et al., 2009) have *likely* reversed that trend (e.g., Koch et al., 2011; Skeie et al., 2011b; Lee et al., 2013). Cryospheric feedbacks and atmospheric dynamical responses in models have an associated poleward shift in the temperature response to aerosol–cloud interactions (Kristjansson et al., 2005; Koch et al., 2009a; Chen et al., 2010).

Solar spectral (UV) irradiance variations along the solar cycle induce ozone responses by modifying the ozone production rate through photolysis of molecular oxygen (Section 8.4.1.4.1), and the resulting differential heating can drive circulation anomalies that lead to regional temperature and precipitation changes (Haigh, 1999; Shindell et al., 2006b; Frame and Gray, 2010; Gray et al., 2010). Such solar forcing may influence natural modes of circulation such as the Northern Annular Mode (e.g., Shindell et al., 2001; de la Torre et al., 2006; Ineson et al., 2011), the South Asian Summer Monsoon (Fan et al., 2009), the Southern Annular Mode (Kuroda and Kodera, 2005; Roscoe and Haigh, 2007) or the ENSO (Mann et al., 2005). The pattern of temperature response is less uniform than the forcing, for example, warming in the NH, but little response in the SH due to temperature moderation by wind speed enhancement effects on ocean circulation (Swingedouw et al., 2011). Regional responses to solar forcing are mediated by the stratosphere, so that reproducing such change requires spectrally varying solar forcing rather than TSI forcing (Lee et al., 2009; Section 8.4.1.4).

Stratospheric aerosol clouds (also Section 8.4.2.2) from tropical eruptions spread poleward and can cover an entire hemisphere or the globe, depending on the initial latitudinal spread. The aerosol eruption cloud from the 1963 Agung was confined mainly to the SH; the 1982 El Chichón mainly to the NH; and the 1991 Pinatubo covered the globe, all with an *e*-folding lifetime of about 1 year (e.g., Antuña et al., 2003). High-latitude eruptions typically stay confined to the high-latitude regions with shorter lifetimes of 2 to 4 months (Kravitz and Robock, 2011). Volcanic aerosols primarily scatter solar radiation back to space, but also absorb longwave radiation with the former larger by an order of magnitude. Stratospheric aerosol absorption heats the layer where they reside and produces distinct vertical and horizontal distributions of the heating rate. The temperature and chemical effects of the aerosols also enhance ozone destruction, which somewhat counteracts the radiative heating (Stenchikov et al., 2002). For tropical eruptions, this may affect atmospheric dynamics, with a stronger polar vortex, a positive mode of the Arctic Oscillation, and winter warming over NH continents (Robock, 2000). Climate responses to solar and volcanic forcings are further discussed in the context of detection and attribution of millennial climate change (see Section 10.7).

The study of how climate responds to regionally varying patterns of forcing is critical for understanding how local activities impact regional

climate; however, the studies are exploratory and generally evoke *very low confidence*. However there is *medium* to *high confidence* in some qualitative but robust features, such as the damped warming of the NH and shifting of the ITCZ from aerosols, and positive feedbacks from high-latitude snow and ice albedo changes.

8.6.3 Spatial Evolution of Radiative Forcing and Response for the Future

Most components of aerosols and ozone precursors are estimated to decrease toward the end of this century in the RCPs except CH_4 in RCP8.5 (Figure 8.2) and nitrate aerosols, though some species reach the maximum amounts of emissions around the mid-21st century (Figure 8.2). The RCPs therefore contrast with the emission scenarios for TAR and AR4, which were based on Special Report on Emissions Scenarios (SRES) and have future projections of larger increase in the near-term climate forcers (NTCFs). It has been questioned whether such low emission of NTCFs is possible in the future given the current policies (Pozzer et al., 2012). This section surveys spatial differences in the RF of aerosols and ozone for the future based on the RCPs.

Figure 8.26 shows the global distributions of changes in aerosol and ozone forcings in 2030 and 2100 relative to 2000 for RCP2.6 and 8.5 (Shindell et al., 2013c). Both scenarios indicate reduced aerosol loading, and thus positive forcing over Europe, North America and Asia by 2100 where RF is above +0.5 W m^{-2} because of substantial reduction of scattering aerosols. The global mean RF due to aerosol–radiation interaction is estimated to be +0.12 and +0.08 W m^{-2} for RCP2.6 and 8.5, respectively, in 2100. Though the RF by total anthropogenic aerosols is positive, reduced BC contributes substantial negative forcing especially over the similar regions. The global mean carbonaceous RF including both the effects of BC and OC is estimated to be –0.20 and –0.11 W m^{-2} for RCP2.6 and 8.5, respectively, in 2100. Early in the century, on the other hand, both scenarios indicate increased negative aerosol forcing over South Asia, with reversal between 2030 and 2100. Emissions of BC, OC and SO_2 will reach their maximums early and middle in the century for RCP2.6 and 8.5, respectively in India. In RCP6, high emission levels of SO_2 in China persist until the mid-21st century (Supplementary Material Figure 8.SM.1), and then it is predicted to keep a high negative RF due to aerosol–radiation interaction over East Asia. The RF due to aerosol–radiation interaction for carbonaceous aerosol is positive over East and South Asia in 2030 relative to 2000 for RCP8.5 because BC emission is also larger in 2030. Over central and southern Africa, a change in the future RF due to aerosol–radiation interaction based on RCPs is not clear mainly because of uncertainties in the wildfires emissions (see Section 7.3.5.3). The global mean total RF due to aerosol–radiation interaction in the future is rather small due to offsetting effects, with reductions in BC, increases in nitrate aerosols, and reductions in scattering aerosols each causing substantially more forcing than the net.

Emissions and atmospheric loadings of natural aerosols are affected by climate change. There is, however, no consensus among studies on future trends of their changes for major natural aerosols, mineral dust and sea salt, as indicated in Section 7.3.5.1. The spatial pattern of the aerosol forcing may be influenced by natural aerosols due to reduction in sea ice cover leading to increased emission of high-latitude sea salt (Struthers et al., 2011; Takemura, 2012) and SOA from vegetation changes (Tsigaridis and Kanakidou, 2007).

The simulations applying the RCPs indicate that the latitude of maximum emission of NTCFs, and therefore of maximum RF, is projected to shift somewhat southward for the next few decades (in 2030 of Figure 8.26). The shift of peak aerosol loading southward is expected to cause the ITCZ to continue to shift northward. This, in combination with warming and drying over tropical land, has been modelled to lead to greatly enhanced drought conditions in the Amazon (Cox et al., 2008). On the other hand, if the low-latitude aerosol is sufficiently absorbing, broadening of the ITCZ convergence region and enhanced cloud cover could result, as modelled for dust (Perlwitz and Miller, 2010).

Reductions in high-latitude BC are expected to contribute to reducing Arctic forcing (e.g., Koch et al., 2011), due to reduction in BC deposition on snow as well as in absorption of sunlight over bright surface. On the other hand, reduction in mid-high-latitude scattering aerosols may offset all or part of the impact of the local Arctic forcing change (Shindell et al., 2010; Koch et al., 2011).

Figure 8.26 also shows the ozone RF in 2030 and 2100 relative to 2000, which includes changes both in tropospheric and stratospheric ozone. Recovery of ozone in the stratosphere in the 21st century will result in positive forcing in the SH high latitudes in comparison with the year 2000 for both the pathways. This is because of the reduced emissions of ozone-depleting substances controlled under the Montreal Protocol, with a small additional effect from a feedback of changes in temperature and in the vertical circulation due to changes in stratospheric compositions (Kawase et al., 2011; Lamarque et al., 2011). In the troposphere, on the other hand, a large difference in the CH_4 emissions between RCP8.5 and the other pathways shown in Figure 8.2 leads to a different RF trend outside the SH high latitudes. Ozone recovery in the stratosphere and ozone increase in the troposphere leads to a positive RF all over the globe in RCP8.5 with a mean of +0.26 W m^{-2} in 2100. The cancellation between positive RF due to ozone increase in the stratosphere and negative RF due to ozone decrease in the troposphere results in a global mean RF of –0.12 W m^{-2} in RCP2.6.

Figure 8.26 also shows the global distributions of changes in ERF due to both aerosol–radiation and aerosol–cloud interactions in 2030 and 2100 relative to 2000 for RCP8.5. Although the ERF includes rapid adjustments and therefore its magnitude is much larger than that of RF due to aerosol–radiation interaction, the spatial pattern is generally similar to RF. The ERF in 2100 shows positive values relative to 2000 in North America, Europe and Asia even with RCP8.5, which indicates the aerosol forcing is projected to approach to the pre-industrial level.